Published in final edited form as:
Curr Opin Hematol. 2007 May ; 14(3): 183–190. doi:10.1097/MOH.0b013e3280d2b76b.

Magnetic resonance imaging measurement of iron overload

John C. Wood
Divisions of Pediatric Cardiology and Radiology, Children's Hospital Los Angeles, Los Angeles, California, USA

Abstract

Purpose of review—To highlight recent advances in magnetic resonance imaging estimation of somatic iron overload. This review will discuss the need and principles of magnetic resonance imaging-based iron measurements, the validation of liver and cardiac iron measurements, and the key institutional requirements for implementation.

Recent findings—Magnetic resonance imaging assessment of liver and cardiac iron has achieved critical levels of availability, utility, and validity to serve as the primary endpoint of clinical trials. Calibration curves for the magnetic resonance imaging parameters R2 and R2* (or their reciprocals, T2 and T2*) have been developed for the liver and the heart. Interscanner variability for these techniques has proven to be on the order of 5–7%.

Summary—Magnetic resonance imaging assessment of tissue iron is becoming increasingly important in the management of transfusional iron load because it is noninvasive, relatively widely available and offers a window into presymptomatic organ dysfunction. The techniques are highly reproducible within and across machines and have been chemically validated in the liver and the heart. These techniques will become the standard of care as industry begins to support the acquisition and postprocessing software.

Keywords

heart; iron overload; liver; magnetic resonance imaging; thalassemia

Introduction

Significant progress in magnetic resonance imaging (MRI) quantitation has occurred since a National Institute of Diabetes and Digestive and Kidney Diseases (NIDDK) workshop in 1991, but the consensus statement from that meeting serves as a good reference for prior work [1]. The present article focuses on the use of MRI to quantitate organ iron burden in systemic iron overload disorders. Supporting validation studies for liver and cardiac iron calibration are presented as well as examples demonstrating integration of the new techniques into clinical practice.

Utility of liver iron estimates

Patients with thalassemia major and other transfusion-dependent anemias receive roughly 0.4 mg/kg/day of heme iron, nearly 50 times the physiologic rate of iron absorption [2,3]. Without aggressive iron chelation therapy, these patients die from endocrine and cardiac complications in the second decade of life [4]. Chelation therapy is life saving, but requires close monitoring of iron balance [5]. Trends in serum ferritin are useful in tracking chelator responsiveness, are

Correspondence to John C. Wood MD, PhD, Divisions of Pediatric Cardiology and Radiology, Children's Hospital Los Angeles, Mailstop 34, 4650 Sunset Blvd, Los Angeles, CA, 90027 USA, Tel: +1 323 669 5470; fax: +1 323 669 7317; jwood@chla.usc.edu.

relatively inexpensive and are widely available [6–8]. Ferritin values, however, can be confounded by inflammatory state and may give wildly inaccurate estimates of total body iron in selected patients [9,10].

As a result, some thalassemia and sickle cell disease centers have used liver iron concentration by biopsy as their gold standard for chelation titration [11,12]. The liver is the dominant iron storage organ and liver iron concentration correlates closely with the total iron balance [13, 14]. Elevated liver iron also prospectively predicts poor endocrine and cardiovascular outcomes in patients with thalassemia major [14,15].

Unfortunately, liver biopsy is invasive, expensive and subject to sampling error [16–18]. Although the risk of ultrasound-guided liver biopsy is relatively low, hemorrhage requiring prolonged hospitalization occurs in approximately 0.5% of cases [19,20]. Proper sedation and local anesthesia can minimize the discomfort, however postprocedure pain decreases patient acceptance, increasing the ‘effective’ interval between studies. Lastly, the reproducibility of liver iron measurements is poor in diseased livers, limiting its utility for serial measurement [21,22].

To counter the shortcomings of liver biopsy, a number of noninvasive techniques have been applied to liver iron estimation including the superconducting quantum interference device (SQUID) [23,24], quantitative computed tomography (qCT) [25–27], and MRI [28–30]. MRI has clearly emerged as the dominant technique because of its sensitivity, reproducibility [31, 32], availability [33•], and ability to image multiple organs in the body during a single imaging session [34,35]. MRI has been integrated into the standard of care at centers where it is available and it is providing new windows into the pathophysiology of iron overload [36].

Principles of magnetic resonance imaging-based iron measurements

MRI operates like many imaging modalities in that it transmits a signal into the body and creates an image from the signal returning from the body after it has interacted with the microenvironment. With MRI, the transmitted signal is a microwave which excites water protons in the body to higher magnetic energy states. As these water protons relax back to the unexcited state, they emit microwaves that are received and interpreted by the scanner; these waves reflect the magnetic milieau near the protons. In noniron overloaded tissues, the magnetic environment is fairly magnetically homogeneous. This means that the signals received from different areas in the tissue remain coherent with one another and the signals last for a long duration (bright images without much contrast). Iron deposits, however, act like little magnets when placed in a strong magnetic field; protons diffusing along different paths experience wildly different magnetic profiles, disrupting coherence among the protons and darkening the image more quickly [37,38].

This process is illustrated in Fig. 1. MRI has the ability to ‘refocus’ the radio waves from the tissues at specific time intervals known as echo times. The longer the echo time (moving from left to right in Fig. 1), the more discordant the proton signals become and the darker the image. Iron overloaded liver (Fig. 1, top panels) simply darkens more quickly with echo time. In fact, this darkening process behaves similarly to radioactive material and can be described by a ‘half life’. The MRI scanner can refocus the returning signal either using a special radiofrequency pulse (forming a so-called spin echo), or by using special small magnets known as gradients (forming a so-called gradient echo). The time constant for a spin echo is known as T2 and for a gradient echo is known as T2*. The greater the tissue iron, the shorter the signal half lives, and the smaller the T2 and T2* become.

Some investigators prefer to report rates of signal decay, R2 or R2*, instead of the half lives T2 or T2*. These distinctions are purely computational and not related to the imaging itself. These rates of signal decay are simply the reciprocals of T2 and T2*:

$$R2 = 1000/T2 \quad (1)$$

$$R2* = 1000/T2* \quad (2)$$

The factor of 1000 is used because T2 and T2* are usually reported in ms and the units of R2 and R2*are Hertz or s^{-1}. So a T2* of 20 ms is equal to an R2 * of 50 Hz and vice versa. The advantage of R2 and R2* notation is that these parameters are directly proportional to iron, rather than inversely proportional to iron; results in the liver are typically reported as R2 and R2* values [28,30] whereas T2 and T2* reporting is more common in the heart [33•,34,35].

Validation of liver iron measurements

Liver R2 and R2* measurements were the first to be calibrated to tissue iron because liver biopsy was routinely obtained in clinical practice. In a study of over 100 patients, St Pierre *et al*. [30] demonstrated a curvilinear relationship between liver iron estimated by R2 and by biopsy (Fig. 2), having a correlation coefficient of 0.98. The prediction error was comparable to the intrinsic variability of liver biopsy. This work followed a number of supporting manuscripts validating the methodology [39–43]. The first R2* results, published by Anderson *et al.* [34], demonstrated a near-linear relationship between liver R2* and biopsy iron in 24 patients. Unfortunately, the study was confounded by a high incidence of liver fibrosis which dramatically increased liver iron concentration variability. Our laboratory followed with a study in hepatitis C negative patients that demonstrated a stronger linear relationship between liver R2* and liver iron [Fig. 3(a)] [28]. Furthermore, using a combination of iron estimates by R2* and by liver biopsy, we were able to closely replicate the St Pierre calibration curve. Figure 3(b) demonstrates an updated figure reflecting 384 simultaneous R2 and R2* determinations in iron overloaded patients. Despite significant differences in signal acquisition and processing there is strong internal consistency among the R2 and R2* techniques.

These data all represent single-echo MRI acquisitions, that is, only one echo time is collected per tissue excitation. Newer MRI scanners can speed R2 and R2* acquisition by acquiring multiple echoes (either gradient echoes or spin echoes) with each excitation. Fortunately, R2* values are nearly identical whether acquired by either technique, allowing comparison of results from old and new scanners [32]. Multiple-echo spin-echo acquisitions exhibit more complicated behavior [37,38]. The calibration curve derived by St Pierre does not apply and observed R2 values are lower than predicted for single-echo measurements [44•,45,46].

R2 and R2* values also scale linearly with magnetic field strength. Although 1.5 T magnets remain the most popular imaging platform, 3 T magnets are becoming increasingly popular. Storey *et al.* [47] demonstrated that cardiac and liver R2* values measured at 3 T are almost exactly double those observed at 1.5 T. High-field R2 measurements have not been similarly validated in humans, although there are excellent data from a marmoset hemosiderosis model showing similar effects [48].

High field imaging may have advantages when tissue iron levels are low and high image resolution is imperative, such as for brain iron quantitation. There are two important disadvantages, however. First, magnetic susceptibility artifacts cause more problems at higher field strength; this is particularly important when organs are near lung, bowel gas, or sinuses.

Second, heavy hepatic iron burden can cause R2 and R2* to increase beyond the limits of detection. Therefore, higher field strengths for cardiac and liver iron estimation should only be used if there is no practical alternative.

Need for target organ assessment

While the liver iron is a good surrogate for total body iron flux, the majority of iron toxicities occur in tissues carrying a trivial proportion of the total somatic iron burden. More importantly, these iron-sensitive 'target' organs have different mechanisms and kinetics of iron uptake/clearance [49–51]. Specifically, endocrine tissue and heart take up circulating labile iron species that are not bound to transferrin (so-called NTBI), while liver iron uptake is predominantly mediated via transferrin [49,50]. As a result, serum ferritin and liver iron values have almost no predictive value for cardiac iron deposition when evaluated on a cross-sectional basis [34,35,52•]. High liver iron values still convey a negative prospective risk [14,15,53], however low liver iron values are not necessarily reassuring. Patients may silently harbor or even accumulate cardiac iron despite apparently adequate chelation as judged by liver iron and serum ferritin values [54,55].

The ability of MRI to detect and monitor the otherwise silent iron infiltration of cardiac tissue has truly revolutionized the management of transfusional iron overload. Figure 4 contrasts two patients with discordant cardiac and liver iron burden. One patient has heavy liver iron load (>60 mg/g dry weight) with no cardiac iron deposition. The second patient exhibits moderate cardiac iron burden with normal hepatic iron levels. The first patient required high-dose chelation therapy to prevent subsequent cardiac iron accumulation. The second patient required continuous deferoxamine therapy to facilitate cardiac iron removal but at low dose to avoid chelator toxicity.

Better insight into the dynamics of liver and heart iron loading can be obtained by serially plotting scattergrams of the two variables. Figure 5(a) demonstrates iron trajectories of five patients. Arrows indicate increasing time and temporal sampling ranging from 6 months to 2 years. The heart loaded quickly during periods of heavy hepatic siderosis but cleared substantially only when liver iron levels were quite low. The trajectories of these patients trace a complete oval, destroying the cross-sectional relationship between liver and cardiac iron.

The apparent hysteresis exhibited by cardiac iron burden suggests that there is a critical liver burden for cardiac iron loading. Figure 5(b), however, demonstrates two important counter examples. Both patients developed cardiac iron loading despite apparently 'safe' levels of liver iron. Similar findings have been observed by others [54,55]. Therefore, while high liver iron and ferritin values are always undesirable, low values do not guarantee cardiac protection.

Validation of cardiac iron measurements

Cardiac T2* was initially received with considerable skepticism [56–58]. Since cardiac biopsy is more variable and more dangerous than hepatic biopsy, direct tissue validation of cardiac T2* was a challenge [59,60]. Animal models represent a logical first step. Our laboratory demonstrated that cardiac R2* (1/T2*) rose linearly with cardiac iron in a gerbil model. Interestingly, liver and cardiac iron calibration curves were quite similar, on a wet weight basis [61]. As a subsequent 'thought experiment', we then extrapolated our human liver R2*–iron calibration curves to the heart T2* data and found that predicted iron levels were consistent with values derived from autopsy. Our studies were followed by gerbil work validating the utility of R2 and magnetic susceptibility measurements [62].

Since iron storage and distribution likely vary between humans and gerbils, we extended our validation studies to include fresh postmortem tissue [63•]. This study exploited the patchy

nature of cardiac iron deposition to correlate variations in cardiac R2 and R2* with variations in tissue iron concentration (Fig. 6). Although it was not possible to characterize the MRI–iron calibration over the entire pathophysiologic range, we were able to demonstrate that R2 and R2* increases (T2 and T2* shortening) reflect cardiac iron deposition in human tissue. Further autopsy studies are ongoing in nearly a dozen specimens to place tighter bounds on the absolute calibration.

Clinically, however, determination of absolute cardiac iron levels is unnecessary; functional correlates suffice. Figure 7 demonstrates the interplay between left ventricular ejection fraction and cardiac T2* in thalassemia major patients. Important points may be summarized as follows: all patients having a normal T2* (>20 ms) had normal ejection fraction; the prevalence of left ventricular dysfunction progressively increased as T2* decreased into the abnormal range; many patients with detectable cardiac iron (T2*<20 ms) nonetheless had normal cardiac function. This implies that abnormal cardiac T2* represents a preclinical degree of cardiac iron loading [34]. Figure 7(b) demonstrates the increasing prevalence of cardiac dysfunction at low T2*in a retrospective analysis of 972 cardiac T2* examinations [64]. Although the data represent a cross-sectional sampling rather than a prospective risk assessment, the implied prospective risk for a patient with low T2* is obvious.

From a practical perspective, we divide patients into three categories based upon their cardiac T2* values. Patients with T2*greater than 20 reside in the ‘green’ zone and iron chelation is guided by trends in their estimated liver iron. Patients with T2* between 10 and 20 reside in the ‘yellow’ zone where cardiac iron deposition has occurred but there is little immediate risk of cardiac decompensation. Patients with T2*<10 ms occupy the ‘red zone’, representing sufficiently increased risk of cardiac decompensation to require immediate review and intensification of chelation therapy.

Other target organ assessments

MRI has also been used to characterize tissue iron deposits in the brain, pituitary gland, bone marrow, kidney and pancreas [65–71]. Although less well validated and clinically exploited, these approaches are likely to become increasingly important in the assessment of transfusional iron overload. The merits and limitations of these investigations are beyond the scope of this review, but several key references are included for interested readers.

Magnetic resonance imaging examinations

MRI has the remarkable ability to evaluate anatomic, physiologic, and chemical data in patients. All iron examinations should measure cardiac and liver iron as well as cardiac function. This portion of the examination can be performed in a half hour imaging slot (15–20 min of imaging time). Our practice is to utilize a full 1 h imaging slot (40 min of imaging time) to characterize liver iron by both R2 and R2* methods, liver volume, pancreatic and kidney R2* as well as cardiac output and diastolic function. Children under 7 years old are typically sedated using propofol infusion. Older patients take no medications unless a benzodiazepine is needed to treat claustrophobia. Since cardiac function is an established, billable procedure, insurance reimbursement has been satisfactory.

Requirements to perform magnetic resonance imaging assessment of liver and cardiac iron

MRI scanners run computer programs called ‘pulse sequences’ necessary to form T2 and T2* images. State-of-the-art, fast iron imaging sequences are available on all major MRI platforms for sites having research agreements. Sites lacking such agreements can also usually obtain

satisfactory iron imaging, but it takes more effort to validate the approach. In fact, the lack of local radiologic experience or incentive is the single greatest barrier to iron quantitation by MRI.

Once proper images are acquired, images must be computer processed to generate the R2 or R2* values. Most sites have developed their own local expertise by contracting physicists or programmers to write the reconstruction algorithms; algorithmic details may be found in several publications [40,42,72•]. Other sites have used commercial software (http://www.cmrtools.com) or services (http://www.ferriscan.com) to generate their iron estimates.

Conclusion

MRI combines accurate, reproducible and platform-robust estimates of organ iron concentration with structural and functional correlations in patients with iron overload. Further work is ongoing to better understand interpatient and interorgan differences in iron loading and unloading. These techniques will become the standard of care as industry begins to support the technical demands of their implementation.

Acknowledgments

This work has been supported by the NIH 5 RO1 HL075592, the General Clinical Research Center (GCRC, RR00043-43), Novartis Pharma, Department of Pediatrics at Children's Hospital Los Angeles, Wright Foundation, and Gunther Foundation.

Abbreviation

MRI	magnetic resonance imaging

References and recommended reading

Papers of particular interest, published within the annual period of review, have been highlighted as:

• of special interest

•• of outstanding interest

Additional references related to this topic can also be found in the Current World Literature section in this issue (p. 291).

1. Brittenham GM, Badman DG. Noninvasive measurement of iron: report of an NIDDK workshop. Blood 2003;101:15–19. [PubMed: 12393526]
2. Gordeuk VR, Bacon BR, Brittenham GM. Iron overload: causes and consequences. Annu Rev Nutr 1987;7:485–508. [PubMed: 3300744]
3. McLaren GD, Muir WA, Kellermeyer RW. Iron overload disorders: natural history, pathogenesis, diagnosis, and therapy. Crit Rev Clin Lab Sci 1983;19:205–266. [PubMed: 6373141]
4. Ehlers KH, Levin AR, Markenson AL, et al. Longitudinal study of cardiac function in thalassemia major. Ann N Y Acad Sci 1980;344:397–404. [PubMed: 6930879]
5. Borgna-Pignatti C, Rugolotto S, De Stefano P, et al. Survival and complications in patients with thalassemia major treated with transfusion and deferoxamine. Haematologica 2004;89:1187–1193. [PubMed: 15477202]
6. Brissot P, Bourel M, Herry D, et al. Assessment of liver iron content in 271 patients: a reevaluation of direct and indirect methods. Gastroenterology 1981;80:557–565. [PubMed: 7450446]

7. Bonkovsky HL, Slaker DP, Bills EB, Wolf DC. Usefulness and limitations of laboratory and hepatic imaging studies in iron-storage disease. Gastroenterology 1990;99:1079–1091. [PubMed: 2394329]
8. Borgna-Pignatti C, Castriota-Scanderbeg A. Methods for evaluating iron stores and efficacy of chelation in transfusional hemosiderosis. Haematologica 1991;76:409–413. [PubMed: 1806447]
9. de Virgiliis S, Sanna G, Cornacchia G, et al. Serum ferritin, liver iron stores, and liver histology in children with thalassaemia. Arch Dis Child 1980;55:43–45. [PubMed: 7377816]
10. Brittenham GM, Cohen AR, McLaren CE, et al. Hepatic iron stores and plasma ferritin concentration in patients with sickle cell anemia and thalassemia major. Am J Hematol 1993;42:81–85. [PubMed: 8416302]
11. Olivieri NF. Progression of iron overload in sickle cell disease. Semin Hematol 2001;38:57–62. [PubMed: 11206962]
12. Olivieri NF, Brittenham GM. Iron-chelating therapy and the treatment of thalassemia. Blood 1997;89:739–761. [PubMed: 9028304]
13. Angelucci E, Brittenham GM, McLaren CE, et al. Hepatic iron concentration and total body iron stores in thalassemia major. N Engl J Med 2000;343:327–331. [PubMed: 10922422]
14. Brittenham GM, Griffith PM, Nienhuis AW, et al. Efficacy of deferoxamine in preventing complications of iron overload in patients with thalassemia major. N Engl J Med 1994;331:567–573. [PubMed: 8047080]
15. Telfer PT, Prestcott E, Holden S, et al. Hepatic iron concentration combined with long-term monitoring of serum ferritin to predict complications of iron overload in thalassaemia major. Br J Haematol 2000;110:971–977. [PubMed: 11054091]
16. Emond MJ, Bronner MP, Carlson TH, et al. Quantitative study of the variability of hepatic iron concentrations. Clin Chem 1999;45:340–346. [PubMed: 10053034]
17. Crisponi G, Ambu R, Cristiani F, et al. Does iron concentration in a liver needle biopsy accurately reflect hepatic iron burden in beta-thalassemia? Clin Chem 2000;46:1185–1188. [PubMed: 10926902]
18. Butensky E, Fischer R, Hudes M, et al. Variability in hepatic iron concentration in percutaneous needle biopsy specimens from patients with transfusional hemosiderosis. Am J Clin Pathol 2005;123:146–152. [PubMed: 15762291]
19. Angelucci E, Baronciani D, Lucarelli G, et al. Needle liver biopsy in thalassaemia: analyses of diagnostic accuracy and safety in 1184 consecutive biopsies. Br J Haematol 1995;89:757–761. [PubMed: 7772512]
20. Janes CH, Lindor KD. Outcome of patients hospitalized for complications after outpatient liver biopsy. Ann Intern Med 1993;118:96–98. [PubMed: 8416324]
21. Ambu R, Crisponi G, Sciot R, et al. Uneven hepatic iron and phosphorus distribution in beta-thalassemia. J Hepatol 1995;23:544–549. [PubMed: 8583142]
22. Villeneuve JP, Bilodeau M, Lepage R, et al. Variability in hepatic iron concentration measurement from needle-biopsy specimens. J Hepatol 1996;25:172–177. [PubMed: 8878778]
23. Nielsen P, Engelhardt R, Duerken M, et al. Using SQUID biomagnetic liver susceptometry in the treatment of thalassemia and other iron loading diseases. Transfus Sci 2000;23:257–258. [PubMed: 11099909]
24. Brittenham GM, Farrell DE, Harris JW, et al. Magnetic-susceptibility measurement of human iron stores. N Engl J Med 1982;307:1671–1675. [PubMed: 7144866]
25. Goldberg HI, Cann CE, Moss AA, et al. Noninvasive quantitation of liver iron in dogs with hemochromatosis using dual-energy CT scanning. Invest Radiol 1982;17:375–380. [PubMed: 7129818]
26. Howard JM, Ghent CN, Carey LS, et al. Diagnostic efficacy of hepatic computed tomography in the detection of body iron overload. Gastroenterology 1983;84:209–215. [PubMed: 6848401]
27. Chapman RW, Williams G, Bydder G, et al. Computed tomography for determining liver iron content in primary haemochromatosis. BMJ 1980;280:440–442. [PubMed: 7370525]
28. Wood JC, Enriquez C, Ghugre N, et al. MRI R2 and R2*mapping accurately estimates hepatic iron concentration in transfusion-dependent thalassemia and sickle cell disease patients. Blood 2005;106:1460–1465. [PubMed: 15860670]

29. Gandon Y, Olivie D, Guyader D, et al. Noninvasive assessment of hepatic iron stores by MRI. Lancet 2004;363:357–362. [PubMed: 15070565]
30. St Pierre TG, Clark PR, Chua-anusorn W, et al. Noninvasive measurement and imaging of liver iron concentrations using proton magnetic resonance. Blood 2005;105:855–861. [PubMed: 15256427]
31. Westwood MA, Anderson LJ, Firmin DN, et al. Interscanner reproducibility of cardiovascular magnetic resonance T2* measurements of tissue iron in thalassemia. J Magn Reson Imaging 2003;18:616–620. [PubMed: 14579406]
32. Westwood M, Anderson LJ, Firmin DN, et al. A single breath-hold multiecho T2*cardiovascular magnetic resonance technique for diagnosis of myocardial iron overload. J Magn Reson Imaging 2003;18:33–39. [PubMed: 12815637]
33•. Tanner MA, He T, Westwood MA, et al. Multicenter validation of the transferability of the magnetic resonance T2* technique for the quantification of tissue iron. Haematologica 2006;91:1388–1391. Demonstrates the intercenter reproducibility of cardiac T2*. [PubMed: 17018390]
34. Anderson LJ, Holden S, Davis B, et al. Cardiovascular T2-star (T2*) magnetic resonance for the early diagnosis of myocardial iron overload. Eur Heart J 2001;22:2171–2179. [PubMed: 11913479]
35. Wood JC, Tyszka JM, Ghugre N, et al. Myocardial iron loading in transfusion-dependent thalassemia and sickle-cell disease. Blood 2004;103:1934–1936. [PubMed: 14630822]
36. Wood JC, Enriquez C, Ghugre N, et al. Physiology and pathophysiology of iron cardiomyopathy in thalassemia. Ann N Y Acad Sci 2005;1054:386–395. [PubMed: 16339687]
37. Wood JC, Fassler J, Meade T. Mimicking liver iron overload using liposomal ferritin preparations. Mag Res Med 2004;51:607–611.
38. Ghugre NR, Coates TD, Nelson MD, Wood JC. Mechanisms of tissue-iron relaxivity: nuclear magnetic resonance studies of human liver biopsy specimens. Magn Reson Med 2005;54:1185–1193. [PubMed: 16215963]
39. Clark PR, St Pierre TG. Quantitative mapping of transverse relaxivity (1/T(2)) in hepatic iron overload: a single spin-echo imaging methodology. Magn Reson Imaging 2000;18:431–438. [PubMed: 10788721]
40. Clark PR, Chua-anusorn W, St Pierre TG. Bi-exponential proton transverse relaxation rate (R2) image analysis using RF field intensity-weighted spin density projection: potential for R2 measurement of iron-loaded liver. Magn Reson Imaging 2003;21:519–530. [PubMed: 12878262]
41. Clark PR, Chua-Anusorn W, St Pierre TG. Proton transverse relaxation rate (R2) images of iron-loaded liver tissue: mapping local tissue iron concentrations with MRI. Magn Reson Med 2003;49:572–575. [PubMed: 12594762]
42. Clark PR, Chua-anusorn W, St Pierre TG. Reduction of respiratory motion artifacts in transverse relaxation rate (R2) images of the liver. Comput Med Imaging Graph 2004;28:69–76. [PubMed: 15127751]
43. Pardoe H, Clark PR, St Pierre TG, et al. A magnetic resonance imaging based method for measurement of tissue iron concentration in liver arterially embolized with ferrimagnetic particles designed for magnetic hyperthermia treatment of tumors. Magn Reson Imaging 2003;21:483–488. [PubMed: 12878257]
44•. Alexopoulou E, Stripeli F, Baras P, et al. R2 relaxometry with MRI for the quantification of tissue iron overload in beta-thalassemic patients. J Magn Reson Imaging 2006;23:163–170. Liver biopsy validation of a multiecho R2 sequence in thalassemia patients. [PubMed: 16374880]
45. Voskaridou E, Douskou M, Terpos E, et al. Magnetic resonance imaging in the evaluation of iron overload in patients with beta thalassaemia and sickle cell disease. Br J Haematol 2004;126:736–742. [PubMed: 15327528]
46. Voskaridou E, Douskou M, Terpos E, et al. Deferiprone as an oral iron chelator in sickle cell disease. Ann Hematol 2005;84:434–440. [PubMed: 15809885]
47. Storey P, Thompson A, et al. R2* imaging of transfusional iron burden at 3T and comparison with 1.5T. J Magn Reson Imaging. (in press).
48. Bulte JW, Miller GF, Vymazal J, et al. Hepatic hemosiderosis in nonhuman primates: quantification of liver iron using different field strengths. Magn Reson Med 1997;37:530–536. [PubMed: 9094074]

49. Oudit GY, Sun H, Trivieri MG, et al. L-type Ca(2+) channels provide a major pathway for iron entry into cardiomyocytes in iron-overload cardiomyopathy. Nat Med 2003;9:1187–1194. [PubMed: 12937413]
50. Oudit GY, Trivieri MG, Khaper N, et al. Role of L-type Ca2+ channels in iron transport and iron-overload cardiomyopathy. J Mol Med 2006;84:349–364. [PubMed: 16604332]
51. Anderson LJ, Westwood MA, Holden S, et al. Myocardial iron clearance during reversal of siderotic cardiomyopathy with intravenous desferrioxamine: a prospective study using T2* cardiovascular magnetic resonance. Br J Haematol 2004;127:348–355. [PubMed: 15491298]
52•. Tanner MA, Galanello R, Dessi C, et al. Myocardial iron loading in patients with thalassemia major on deferoxamine chelation. J Cardiovasc Magn Reson 2006;8:543–547. Large, cross-sectional evaluation of the prevalence of left ventricular dysfunction as a function of cardiac T2*. [PubMed: 16755844]
53. Olivieri NF, Nathan DG, MacMillan JH, et al. Survival in medically treated patients with homozygous beta-thalassemia. N Engl J Med 1994;331:574–578. [PubMed: 8047081]
54. Anderson LJ, Westwood MA, Prescott E, et al. Development of thalassaemic iron overload cardiomyopathy despite low liver iron levels and meticulous compliance to desferrioxamine. Acta Haematol 2006;115:106–108. [PubMed: 16424659]
55. Kolnagou A, Economides C, Eracleous E, Kontoghiorghes GJ. Low serum ferritin levels are misleading for detecting cardiac iron overload and increase the risk of cardiomyopathy in thalassemia patients: the importance of cardiac iron overload monitoring using magnetic resonance imaging T2 and T2*. Hemoglobin 2006;30:219–227. [PubMed: 16798647]
56. Brittenham GM, Nathan DG, Olivieri NF, et al. Deferiprone versus desferrioxamine in thalassaemia, and T2*validation and utility. Lancet 2003;361:183. author reply 183–184. [PubMed: 12531619]
57. Fischer R, Engelhardt R. Deferiprone versus desferrioxamine in thalassaemia, and T2* validation and utility. Lancet 2003;361:182–183. author reply 183–184. [PubMed: 12531618]
58. St Pierre TG, Chua-anusorn W, Webb J, et al. The form of iron oxide deposits in thalassemic tissues varies between different groups of patients: a comparison between Thai beta-thalassemia/hemoglobin E patients and Australian beta-thalassemia patients. Biochim Biophys Acta 1998;1407:51–60. [PubMed: 9639673]
59. Fitchett DH, Coltart DJ, Littler WA, et al. Cardiac involvement in secondary haemochromatosis: a catheter biopsy study and analysis of myocardium. Cardiovasc Res 1980;14:719–724. [PubMed: 7260965]
60. Olson LJ, Edwards WD, McCall JT, et al. Cardiac iron deposition in idiopathic hemochromatosis: histologic and analytic assessment of 14 hearts from autopsy. J Am Coll Cardiol 1987;10:1239–1243. [PubMed: 3680791]
61. Wood JC, Otto-Duessel M, Aguilar M, et al. Cardiac iron determines cardiac T2*, T2, and T1 in the gerbil model of iron cardiomyopathy. Circulation 2005;112:535–543. [PubMed: 16027257]
62. Wang ZJ, Lian L, Chen Q, et al. 1/T2 and magnetic susceptibility measurements in a gerbil cardiac iron overload model. Radiology 2005;234:749–755. [PubMed: 15734931]
63•. Ghugre NR, Enriquez CM, Gonzalez I, et al. MRI detects myocardial iron in the human heart. Magn Reson Med 2006;56:681–686. Chemical validation of T2 and T2* in human tissue. [PubMed: 16888797]
64. Westwood MA, Anderson LJ, Tanner MA, Pennell DJ. The relationship between myocardial iron deposition and left ventricular dysfunction in thalassemia using cardiovascular magnetic resonance. J Cardiovasc Magn Reson 2005;7:46–47.
65. Argyropoulou MI, Metafratzi Z, Kiortsis DN, et al. T2 relaxation rate as an index of pituitary iron overload in patients with beta-thalassemia major. AJR Am J Roentgenol 2000;175:1567–1569. [PubMed: 11090376]
66. Sparacia G, Banco A, Midiri M, Iaia A. MR imaging technique for the diagnosis of pituitary iron overload in patients with transfusion-dependent beta-thalassemia major. AJNR Am J Neuroradiol 1998;19:1905–1907. [PubMed: 9874546]
67. Miszkiel KA, Paley MN, Wilkinson ID, et al. The measurement of R2, R2*and R2′ in HIV-infected patients using the prime sequence as a measure of brain iron deposition. Magn Reson Imaging 1997;15:1113–1119. [PubMed: 9408132]

68. Graham JM, Paley MN, Grunewald RA, et al. Brain iron deposition in Parkinson's disease imaged using the PRIME magnetic resonance sequence. Brain 2000;123 (Pt 12):2423–2431. [PubMed: 11099445]

69. Isokawa M, Kimura F, Matsuki T, et al. Evaluation of bone marrow iron by magnetic resonance imaging. Ann Hematol 1997;74:269–274. [PubMed: 9236511]

70. Drakonaki E, Papakonstantinou O, Maris T, et al. Adrenal glands in beta-thalassemia major: magnetic resonance (MR) imaging features and correlation with iron stores. Eur Radiol 2005;15:2462–2468. [PubMed: 16086182]

71. Ooi GC, Khong PL, Chan GC, et al. Magnetic resonance screening of iron status in transfusion-dependent beta-thalassaemia patients. Br J Haematol 2004;124:385–390. [PubMed: 14717788]

72•. Ghugre NR, Enriquez CM, Coates TD, et al. Improved R2* measurements in myocardial iron overload. J Magn Reson Imaging 2006;23:9–16. Good description of several important T2* processing details. [PubMed: 16329085]

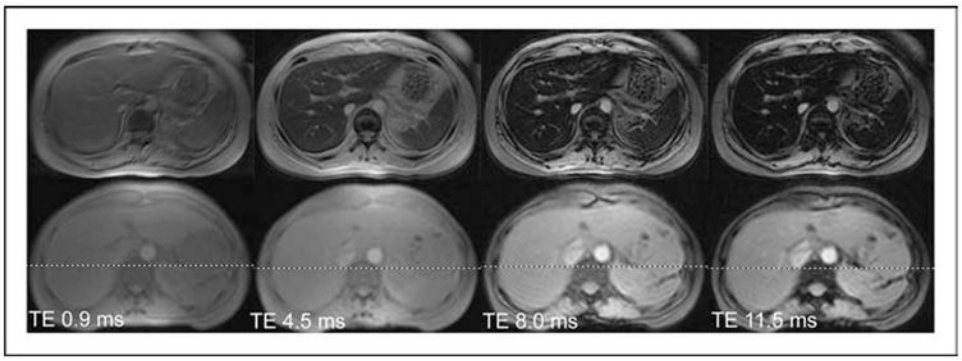

Figure 1. Gradient echo images of liver collected at four different echo times

The top four images were collected from a patient having a liver iron of 6 mg/g. The bottom four images were collected from a normal volunteer. All images darken as the echo time (TE) lengthens, but the iron-heavy tissue darkens faster. The half life of this process is called T2* and the rate is called R2* (R2*=1000/T2*).

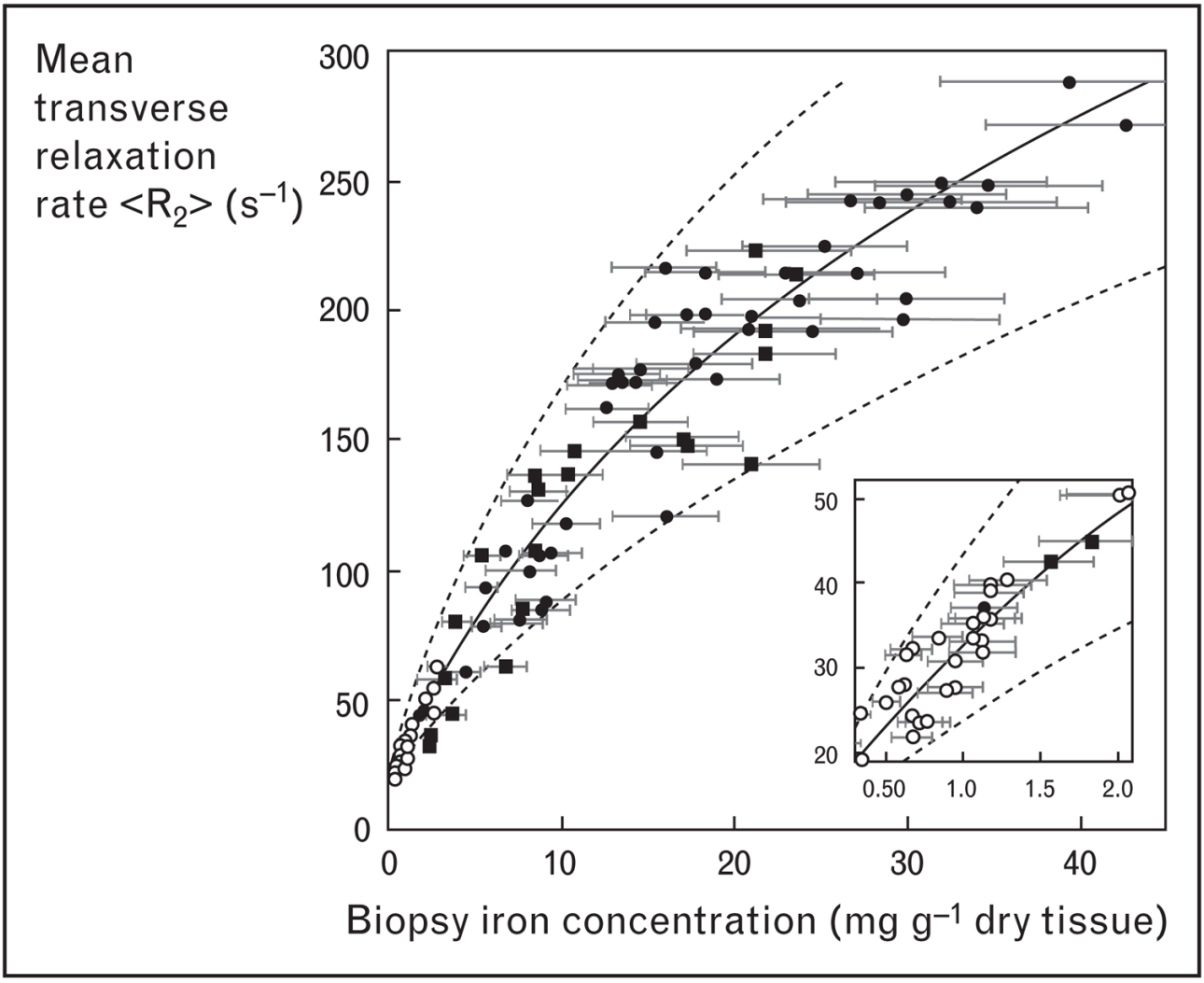

Figure 2. Plot of liver R2 versus biopsied liver iron concentration in 104 patients
Data reproduced with permission from St Pierre [30].

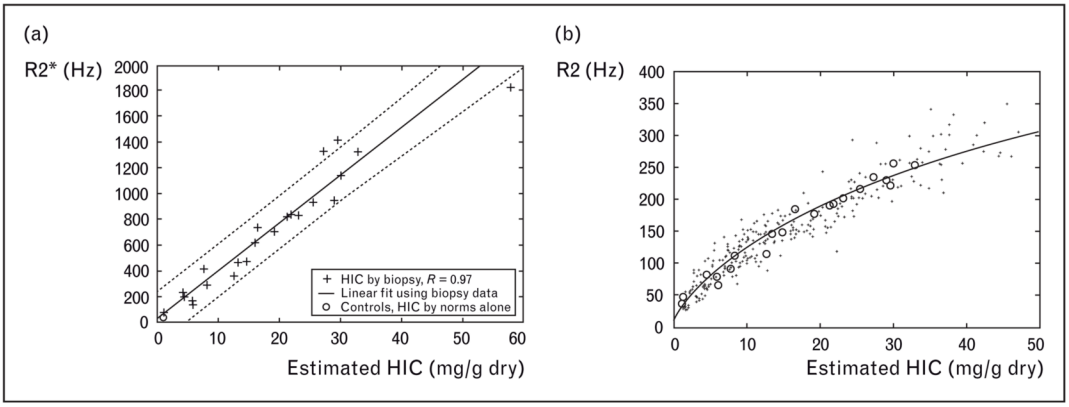

Figure 3. Plots of liver R2 versus biopsied liver iron concentration

(a) Plot of liver R2*versus biopsied liver iron concentration (HIC) in 22 patients. There is a strong linear correlation (r =0.97). (b) Plot of R2 versus liver iron predicted by biopsy (+ signs) or by simultaneously measured R2* HIC estimates (n =384). Bold line represents the Tim St Pierre calibration curve, supporting strong internal consistency between R2 and R2* measurements. This research was originally published in Wood *et al*. [28]. Copyright American Society of Hematology.

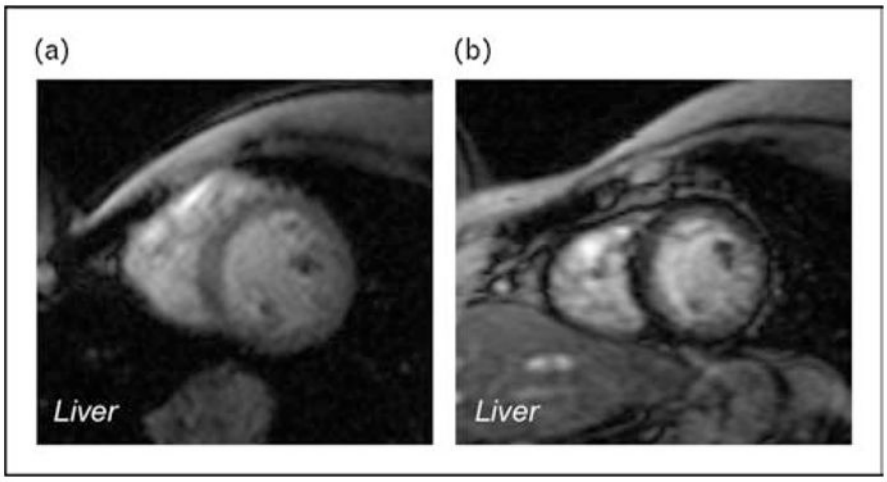

Figure 4. Gradient echo (T2*) imaging illustrating discordant iron loading of the liver and the heart
(a) Heavy liver iron loading (dark tissue) with heart sparing. (b) Heavy cardiac iron loading with no liver iron deposition.

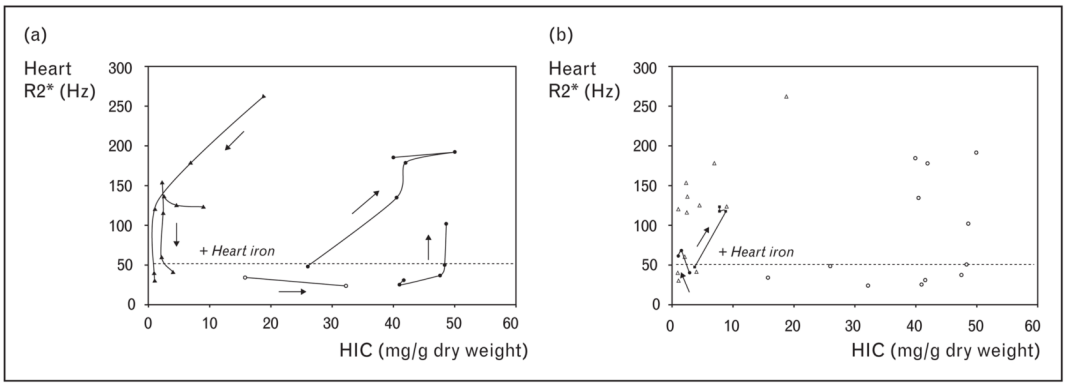

Figure 5. Iron trajectories of five patients

(a) Scattergram demonstrating cardiac iron versus liver iron (HIC) in three patients. Temporal trajectories trace out an oval, demonstrating the lack of cross-sectional correlation between liver and heart iron. (b) Same scattergram with two additional patients who developed cardiac iron loading despite having apparently adequate iron chelation.

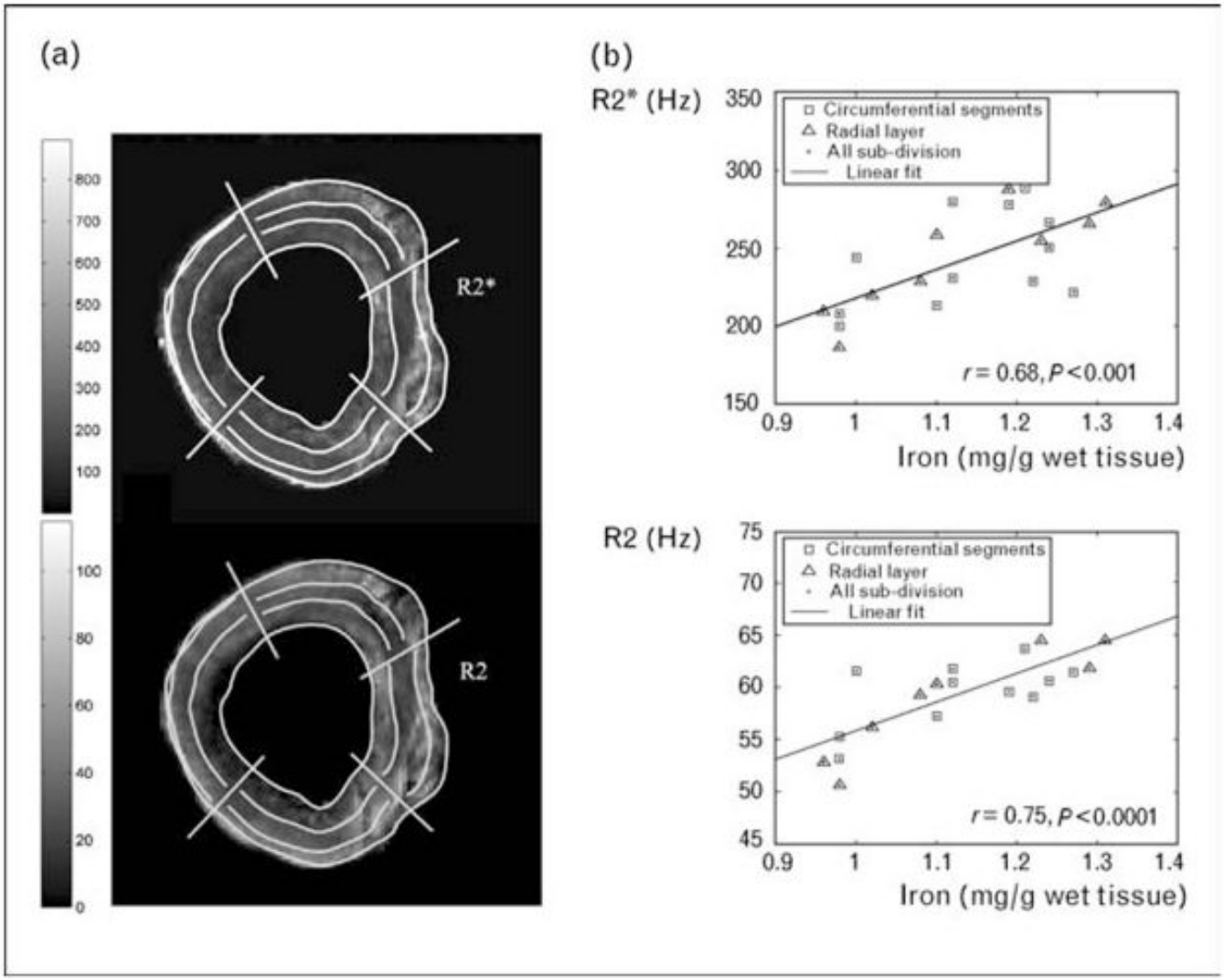

Figure 6. Correlation of variations in cardiac R2 and R2* with variations in tissue iron concentration

(a) R2 and R2*'maps' measured *in vitro* from a fresh postmortem specimen. The grid represents approximate divisions for iron sampling. (b) Rise of R2 and R2* as a function of assayed tissue iron concentration. Graphs redrawn with permission from [63•].

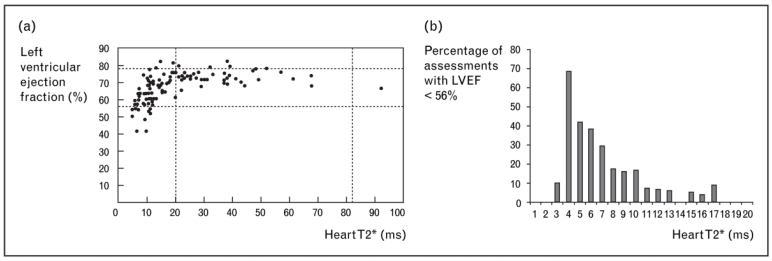

Figure 7. Interplay between left ventricular ejection fraction (LVEF) and cardiac T2* in thalassemia major patients

(a) Plot of LVEF versus cardiac T2* value. Data reproduced with permission from [34]. (b) Prevalence histogram of left ventricular dysfunction (LVEF <56%) as a function of cardiac T2*. Data reproduced with permission from [64].